Progress In Electromagnetics Research, PIER 38, 311–331, 2002

A FULL WAVE THREE DIMENSIONAL ANALYSIS OF FOREST REMOTE SENSING USING VHF ELECTROMAGNETIC WAVE

L. Angot, H. Roussel, and W. Tabbara

Département de Recherche en Électromagnétisme
Laboratoire des Signaux et Systèmes
Supélec, 3 rue Joliot-Curie, Plateau de Moulon
F-91192 Gif-sur-Yvette Cedex, France

Abstract—A forest made of an infinite biperiodic array of trees over a lossy ground, is illuminated by a linearly polarized electromagnetic plane wave in the range of 20 to 90 MHz. Due to the ratio of the wavelength to the array period, only the specular mode is propagative. Therefore, a reflection coefficient is computed and not a backscattering coefficient. It is obtained by means of a full wave approach, based on an integral representation of the electric field. This approach takes into account all possible interactions between each component of the medium as well as ground penetration and provides full information on the phase of the scattered field. Two models of the forest are developed, the two layers one where trees are separated and the four layers one whee the canopy is replaced by an equivalent homogeneous medium. The low frequency (VHF) used here make this homogenization possible and allows one to consider trees with simple shape, the wave being unable to sense details of a tree.

1. INTRODUCTION

Radar remote sensing of forested areas have been investigated since many years. At high frequencies (C, L and P band) these investigations show some limitations as for example in estimating forest biomass parameters, and also a saturation of the backscattered signal [1–3] and [4]. At VHF frequencies, as with the Swedish CARABAS SAR system which operates in the 20–90 MHz band [5, 6] and [7], the electromagnetic wave crosses the canopy and then we have to consider the interaction of the wave with the trunks and the ground. Consequently the scattered field is correlated to the overall biomass of the forest and not only to the biomass located in the upper layers. Moreover, at VHF frequencies, the penetration of the wave through the canopy allows a better detection and characterization of hidden objects. Modelling the interaction of an electromagnetic wave with a forest by means of a full-wave approach seemed tough to be achieved due to the complexity of the studied medium. Models based on the radiative transfer theory (RT) were so far used, but they have shown their limits towards low frequencies, and they only provide intensity informatics. Conventional RT theory ignores the phase of the field interacting with scatterers, which may play an important role especially when large structures as tree trunks are involved. In [8], the phase of the field scattered from each component of the tree is incorporated in the radiative transfer theory, but the result remains

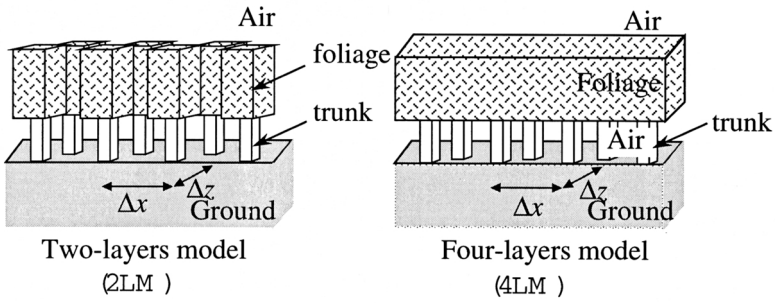

Figure 1. The two considered representations of a forested area.

free from the phase of the field and moreover the interaction between trees themselves and between trees and the ground are not taken into account. Hence an approach based on full-wave method is justified. An example is given by Israelsson [9] who used the FDTD to model, at VHF frequencies, the interactions between the trunk and the branches of a tree placed above a ground. His results show the significant contribution of the coherent interaction between the tree and the ground. Thus, all types of interactions must be taken into account in a full-wave model at VHF frequencies.

In this paper an integral representation, which involves the Green's function of a multilayered medium, is used to determine the field scattered by a forested area illuminated by a VIIF plane wave. The calculation of the scattered field using a full wave model is possible with a simplified representation of the forest. Since we consider the VHF band each tree doesn't need to be described in detail because the wavelength of the incident wave is large when compared with the size of the trunk, and the foliage can be considered as a homogeneous medium. We consider two different models, representing the forested area as a bi-periodic structure placed above a semi-infinite ground plane. Both representations are shown in Figure 1, in the one at the(left, the trees are separate and their foliage replaced by an equivalent homogeneous medium. In the model on the right the canopy is replaced by a single equivalent homogeneous medium. These models are respectively named 2LM for the two layered medium, and 4LM for four layered medium. To calculate the scattered field by the forest, we solve the integral equation obtained for the electric field with a Method of Moment (MoM).†

† This work has been done with the financial support of the French Space Agency (CNES) and the DGA of the french ministery of Defence.

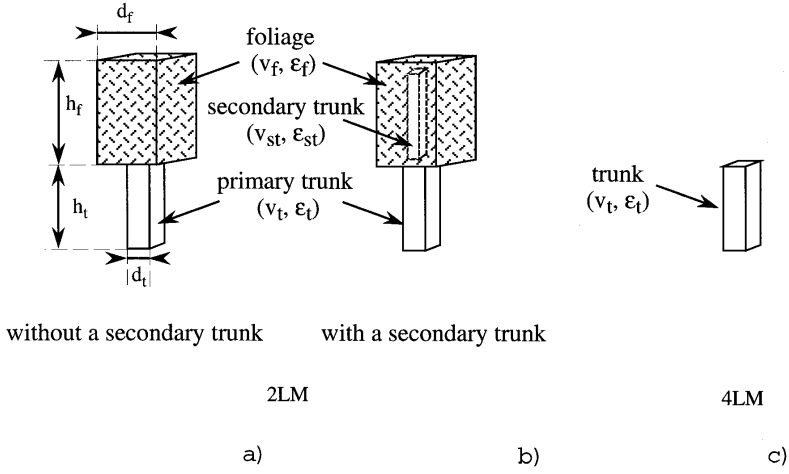

Figure 2. Representation of the reference patterns of the gratings for the 2LM and the 4LM.

2. REPRESENTATIONS OF A FORESTED AREA: 2LM AND 4LM

2.1. The Geometry

The forest is represented by the models 2LM and 4LM of Fig. 1, where in both cases we have a biperiodic grating, the reference patterns of which are those shown on Fig. 2(a) and 2(b) for the 2LM and 2(c) for the 4LM. In the 2LM model we have an array of trees standing over the interface of a two layered medium: air and ground. In the 4LM case we have an array of trunks placed in a four layered medium: air; homogenized foliage layer; air, where the trunks are placed and ground. The array periods are Δx and Δz. The roughness of the ground is considered to be small with respect to the wavelength, and the ground surface is then assumed to be a plane. The incident plane wave is defined on Fig. 3. The plane of incidence is perpendicular to the layers and makes the angle φ with respect to the x-axis of the global coordinate system (x, y, z). The angle of incidence is θ as shown on Fig. 3. We consider the two basic linear polarizations, TM when the electric field is perpendicular to the plane of incidence, and TE when it is in the plane of incidence. In the following, the layered media illuminated by the incident plane wave as shown on Fig. 3(a) and 3(b) with the arrays of trees (2LM) or trunks (4LM) removed, are named the reference problems.

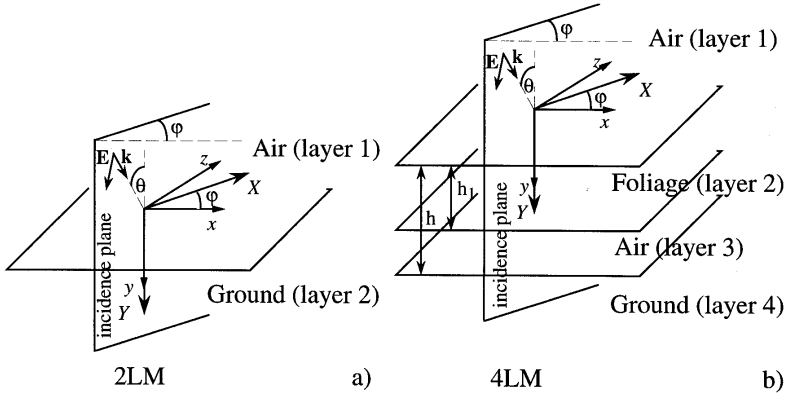

Figure 3. Representation of the reference multilayered media used for the 2LM and the 4LM.

Table 1. Geometrical characteristics of the trees with respect to the age of the forest (A = age (years), = trunk height (m), d_t = trunk side (m), h_{st} = secondary trunk height (m), d_{st} = secondary trunk side (m), h_f = foliage height (m), d_f = foliage side (m), $\Delta = \Delta x = \Delta z =$ period of the gratings (m)).

A	h_t	d_t	h_{st}	d_{st}	h_f	d_f	Δ
6	0.5	0.05	4.5	0.036	4.5	2	2.96
14	4	0.08	5.5	0.04	5.5	2	3.45
22	6,46	0.095	6	0.045	6	3	4.05
30	8.8	0.11	6.5	0.048	6.5	3	4.7
38	11.25	0.125	7	0.049	7	4	5.5
46	13.8	0.138	7.5	0.05	7.5	4	6.45

2.2. The Parameters of the Forested Area

The studied site is a pine tree forest from Les lands in southwest of France. Characteristics of the trees are obtained from [10] and are summarized in Table 1. In the 2LM model we have also considered the case where the trunk penetrates into the foliage (see Fig. 2(b)). This secondary trunk is characterized by its height (h_{St}) and its side (d_{st}) We considered this representation in order to analyze the influence of the model of the tree on the scattered field. In the 4LM model, the height of the foliage layer (noted h_1) is equal to h_f and h is the sum of h_f and h_t. For both models the trunk and the ground

plane are assumed to be isotropic homogeneous media. The relative permittivity of wood, ϵ_t, is equal to $30 + j14$ in the VHF band [11]. To our knowledge, no measured values (or model) of the permittivity of the ground, ϵ_g, are available at low frequencies. We have extrapolated the values given in [12] at 300 MHz and obtained $\epsilon_g = 10 + j3.6$. To determine the permittivity of the foliage, we consider this domain as an inhomogeneous medium made of inclusions (needles and branches) placed in air. The Polder-Van Santen/de Loor formula (1) gives the relative permittivity, $\varepsilon_m = \varepsilon'_m + j\varepsilon''_m$, of the equivalent homogeneous medium [13].

$$\begin{aligned} \varepsilon'_m &= \varepsilon_h \left(1 + \frac{3d_i \left[(\varepsilon'_i - \varepsilon_h)(\varepsilon'_i + 2\varepsilon_h) + (\varepsilon''_i)^2 \right]}{(\varepsilon'_i + 2\varepsilon_h)^2 + (\varepsilon''_i)^2} \right) \\ \varepsilon''_m &= \frac{9 d_i \varepsilon''_i \varepsilon_h^2}{(\varepsilon'_i + 2\varepsilon_h)^2 + (\varepsilon''_i)^2} \end{aligned} \tag{1}$$

Where ϵ_h is the permittivity of the host medium (air) and ϵ_i that of the inclusions (needles and branches). The main contribution of the inclusions is due to the branches, thus the permittivity ϵ_i is equal to ϵ_t. d_i represents the density of inclusions. In our model there is no depolarization of the wave in this medium, because the needles and the branches are represented by spheres. This approximation is justified by the choice of a large wavelength in comparison with the size of these small inclusions. In Table 2, we give the values of the relative permittivities obtained for both models and different ages of the trees.

3. FORMULATION

The integral representation of the total field, obtained when the incident wave is scattered by the forest, is build in a three steps process.

3.1. Step 1: The Reference Field

Here we solve analytically the problem of the interaction of a plane wave with a multilayered medium. For both models, 2LM and 4LM, the reference field for the TM polarization is given by:

$$\begin{aligned} E_z^r(x,y) &= e^{jk_{1x}x} \left(e^{jk_{1y}y} + R_{12} e^{-jk_{1y}y} \right) \textit{layer } 1 \\ E_z^r(x,y) &= e^{jk_{1x}x} \left(T_{(i-1)i} e^{jk_{iy}y} + R_{i(i+1)} e^{-jk_{iy}y} \right) \textit{layer } i \end{aligned} \tag{2}$$

with $i = 2$ (2LM) and $i = 2, 3, 4$ (4LM), where $T_{(i-1)i}$ is the transmission coefficient between layer $i-1$ and i, and $R_{i(i+1)}$ is the

Table 2. Relative permittivity of the foliage with respect to the age of the forest for both models (A = age (years), d_{i2LM} = density of inclusions for the 2LM model, ε'_{m2LM} = real part of the relative permittivity of the homogeneous foliage for the 2LM model, ε''_{m2LM} = imaginary part of the relative permittivity of the homogeneous foliage for the 2LM model, d_{i4LM} = density of inclusions for the 4LM model, ε'_{m4LM} = real part of the relative permittivity of the homogeneous foliage for the 4LM model, ε''_{m4LM} = imaginary part of the relative permittivity y of the homogeneous foliage for the 4LM model).

A	d_{i2LM}	ε'_{m2LM}	ε''_{m2LM}	d_{i4LM}	ε'_{m4LM}	ε''_{m4LM}
6	0.002487	1.00687	2.57e-4	0.001449	1.004	1.496e-04
14	0.002513	1.00694	2.59e-4	0.001328	1.00367	1.372e-04
22	0.002238	1.00619	2.311e-4	0.001263	1.00349	1.304e-04
30	0.001983	1.00548	2.048e-4	0.001137	1.00314	1.174e-04
38	0.001868	1.00516	1.929e-4	0.000982	1.00271	1.014e-04
46	0.001841	1.00508	1.901e-4	0.000833	1.00230	8.604e-05

reflection coefficient between layers i and $i+1$ (for the last layer of the model this coefficient is equal to zero). Similarly we obtain the two components $E^r_x(x,y)$ and $E^r_y(x,y)$ of the electric field, when we consider the TE polarization.

3.2. Step 2: Green's Function of the Multilayered Media

$\overline{\overline{G}}_{iLM}$ is the periodic dyadic Green's functions of the multilayered media (see Figure 3), equal to the potential produced by an array of elementary electric dipoles placed in the same layer as the trees (2LM) or the trunks (4LM). The periods of the array are Δx, Δz. This periodic dyadic Green's function is related to the non periodic one, noted $\overline{\overline{G}}_{ilm}$ which satisfies:

$$\begin{aligned} \Delta\overline{\overline{G}}_{i\ lm}(r,r') + k_i^2\overline{\overline{G}}_{i\ lm}(r,r') &= -\overline{\overline{I}}(r,r')\delta(r,r') \quad \text{for } i = NL-1 \\ &= 0 \quad \text{for } i \neq NL-1 \end{aligned} \tag{3}$$

with $r' = (x', y', z')$ and $r = (x, y, z)$, and the radiation condition and the boundary conditions at the plane interfaces: $y = 0$ for the 2LM and $y = 0$, $h1$ and h for the 4LM. $\overline{\overline{I}}$ is the unit dyad. NL is the number of layers of the considered model (2 or 4). The spectral solution of (3),

noted $\overline{\overline{G}}^{s}_{i\,lm}(\nu,\eta,y,y')$ is related to $\overline{\overline{G}}_{ilm}(r,r')$ by:

$$\overline{\overline{G}}^{s}_{i\ lm}(\nu,\eta,y,y') = \int_{-\infty}^{+\infty}\int_{-\infty}^{+\infty}\overline{\overline{G}}_{i\ lm}(x,y,z,x',y',z') \times \exp -j2\pi(\nu x+\eta z)dxdz \quad (4)$$

The periodic dyadic Green's function is obtained by using Floquet's theorem and is given

$$\overline{\overline{G}}_{i\ LM}(r,r') = \frac{1}{\Delta x\Delta z}\sum_{m=-\infty}^{+\infty}\sum_{n=-\infty}^{+\infty}\overline{\overline{g}}_{i\ lm}(\nu_n,\eta_m,y,y') \times \exp\left(j2\pi\nu_n(x-x')\right)\ \exp\left(j2\pi\eta_m(z-z')\right) \quad (5)$$

with

$$2\pi\nu_n = k_{1x}+\frac{2\pi n}{\Delta x},\quad 2\pi\eta_m = k_{1z}+\frac{2\pi m}{\Delta z} \quad (6)$$

The analytical values of $\overline{\overline{g}}_{i\ lm}$ are given in Appendix A.

3.3. Step 3: The Diffracted Field

By making use of the theory of distributions [14], the field diffracted by the forest, in layer i, is given by:

$$\vec{E}^{d}(r) = [\nabla\cdot\nabla_r + k_i^2]\iiint_{\Omega}\Delta\varepsilon_i(r')\overline{\overline{G}}_{i\ LM}(r,r')\vec{E}(r')dr' \quad (7)$$

where

$$\Delta\varepsilon_i(r') = \frac{\varepsilon(r')-\varepsilon_{(NL-1)}(r')}{\varepsilon_i} \quad (8)$$

Ω represents the domain occupied by the reference pattern of the array.

3.4. Resolution of the Integral Equation by a Method of Moment

Considering the previous results, the integral representation of the total electric field is given

$$\vec{E}(r) = \vec{E}^{r}(r) + [\nabla\cdot\nabla_r + k_i^2]\iiint_{\Omega}\Delta\varepsilon_i(r')\overline{\overline{G}}_{i\ LM}(r,r')\vec{E}(r')dr' \quad (9)$$

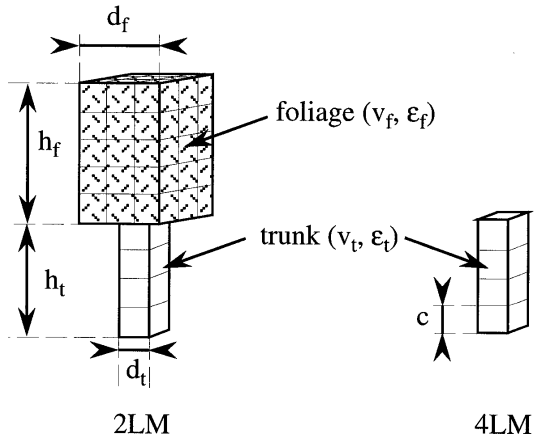

Figure 4. Decomposition of the elementary pattern into cubic sub-cell.

A method of moment is applied to solve this equation by placing r in the volume Ω, occupied by the elementary pattern of the grating. The expansion functions are rectangular pulse functions and the test functions are Dirac's delta distributions [15] and [16]. The elementary pattern of the gratings are divided into cubic sub-cells, Ω_i of side c equal to $\lambda_{cell}/20$. In each sub-cell the electric field and the relative permittivity are assumed having constant values (see Figure 4).

If N is the total number of sub-cells, we obtain a system of linear equations of order $3N$ which is given by:

$$\sum_{q=1}^{3}\sum_{k=1}^{N}\left\{\left(I_{pq}^{kj}-\delta_{kj}\delta pq\right)W_q(\mathbf{r}_k)\right\}=-W_p^r(\mathbf{r}_j) \tag{10}$$

with

$$\vec{W}(r_k)=\begin{pmatrix}E_x(r_k)\\E_y(r_k)\\E_z(r_k)\end{pmatrix},\quad \vec{W}^r(r_j)=\begin{pmatrix}E_x^r(r_j)\\E_y^r(r_j)\\E_z^r(r_j)\end{pmatrix} \tag{11}$$

The 3×3 matrix $[I^{kj}]$ is given in Appendix B. When we consider the diagonal elements of $[I^{kj}]$ $(k=j)$, we have to deal with the singularity of the Green's function. The integrals are then replaced by their principal values [17]. A fast convergence (i.e., n and $m<20$) of the series involved in $[I^{kj}]$ elements is obtained whenever $y_k\neq y_j$, But when $Y_k=y_j$, the convergence is very slow and the summation

of the series given in the calculation of $[I^{kj}]$ requires too many terms (n and $m > 10^4$). To overcome this numerical difficulty, the Green's functions are split into the sum of two terms. The first one is the Green's function of the free space, and is computed by means of a convergence acceleration algorithm introduced by Singh et al. [18]. The second one reduces to a rapidly convergent series [19]. The solution of the linear system (10) gives the values of the three components of the total field inside each sub-cell. Then (9) allows the calculation of the total field at any point in space.

3.5. Calculation of the Reflection Coefficient R

Knowing the total field inside each-subcell of the elementary pattern of the grating, the diffracted field at a point r is given by (7). Due to the ratio of the wavelength to the array period (Δx and Δz), only the specular mode of the diffracted field is propagative. Therefore the results presented in Section4, give the reflection coefficient of the forested area and not the backscattering coefficient. To determine the reflection coefficient, noted R, we have first to calculate the reflected field, which is the sum of the diffracted field in the specular direction and the specular reflection of the multilayered medium deduced from (2) and is given by:

$$\vec{E}^{reflected}(r) = \vec{E}^{d}(r) + R_{12}e^{j(k_{1x}x - k_{1y}y)}u_z \tag{12}$$

for the TM polarization. Similar result is obtained for the TE polarization. Since the diffracted field can be depolarized, we can obtain both polarizations for the reflected field when the incident one is TM or TE polarized. We then define the reflection coefficient R_{TMorTE} according to the relations (13 and 15).

$$R_{TM} = 20\log_{10}\left|\frac{E_z^{reflected}}{E_z^{inc}}\right| \tag{13}$$

with

$$E_z^{inc} = e^{jk_{1x}x}e^{jk_{1y}y} \tag{14}$$

and

$$R_{TEy} = 20\log_{10}\frac{\left|E_y^{reflected}\right|}{\left|\vec{E}^{inc}\right|}, R_{TEx} = 20\log_{10}\frac{\left|E_x^{reflected}\right|}{\left|\vec{E}^{inc}\right|} \tag{15}$$

with

$$\vec{E}^{inc} = \frac{1}{\omega\varepsilon_0}e^{jk_{1x}x}e^{jk_{1y}y}(k_{1x}u_x + k_{1y}u_y) \tag{16}$$

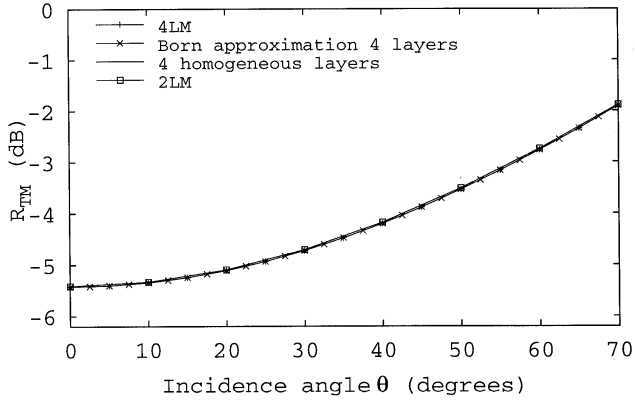

Figure 5. Modulus of the reflected field, R_{TM}, versus incidence angle for a 6 years old tree.

4. NUMERICAL RESULTS

4.1. Validity of the Born Approximation

The exact method described in the previous section requires the knowledge of the total electric field inside the volume Ω of the elementary pattern, whereas with the first-order Born approximation [14] this field is assumed to be the reference field in the 2LM or 4LM. Doing that we avoid calculating the matrix $[I^{kj}]$ and solving the linear system given by (10). Thus, the computation time is considerably reduced since only the diffracted field has to be calculated numerically by means of (7). We also consider the approximate model of a forest made of four homogeneous layers, where the third layer (of the 4LM) is replaced by an equivalent isotropic homogeneous layer obtained by applying the formula (1) to this medium made of wood (trunks) and air. The four models (4LM, Born Approximation, 4 homogeneous layers and 2LM) are applied to the case of a forest made of 6 years old trees. Related amplitude of the reflection coefficient is shown on Figures 5 to 7, for different combinations of the polarizations of the incident and reflected fields versus the angle of incidence of the plane wave illuminating the forested area at a frequency of 20 MHz. We notice that for each polarization the observed variations are the same for the four considered models. This is due to the fact that at 20 MHz, the incident wavelength (15 meters) is large in comparison with the dimensions of the trees. Thus, the main contribution in the calculation of R is the specular reflection of the multilayered medium.

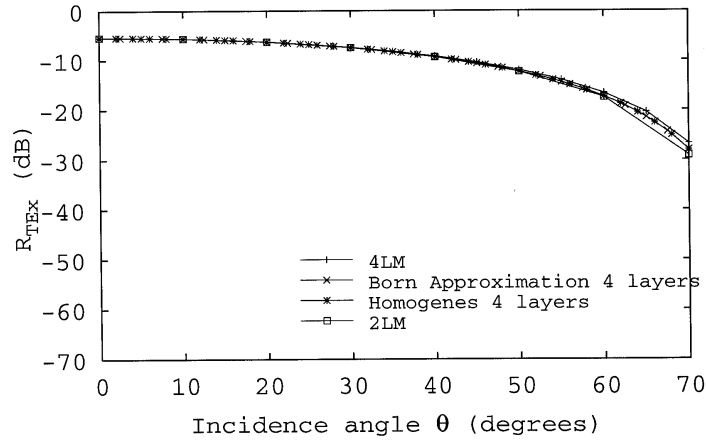

Figure 6. Modulus of the reflected field, R_{TE_x}, versus incidence angle for a 6 years old tree.

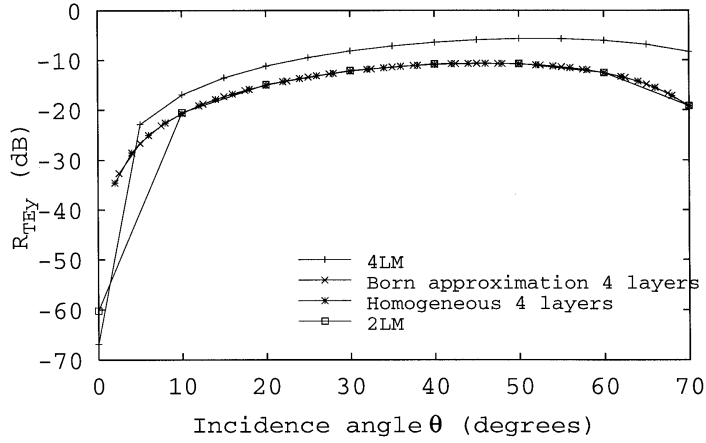

Figure 7. Modulus of the reflected field, R_{TE_y}, versus incidence angle for a 6 years old tree.

If we examine the phase of the reflected field, Fig. 8 and Fig. 9 significant differences appear between the results provided by the four models. The exact models (4LM and 2LM) give similar results with however a phase shift of 50 degrees. It corresponds to a different choice of the origin of phase in the two models (see Fig. 3).

An other important parameter in the model is the frequency of the incident wave. Indeed, if we consider frequencies greater than

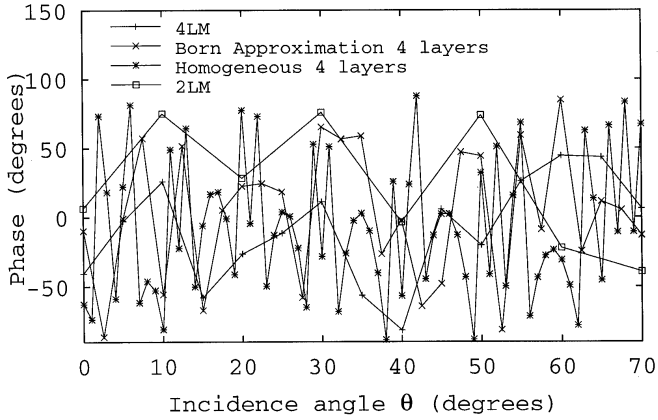

Figure 8. Phase of the reflected field TM case, versus incidence angle for a 6 years old tree when the incident polarization is horizontal.

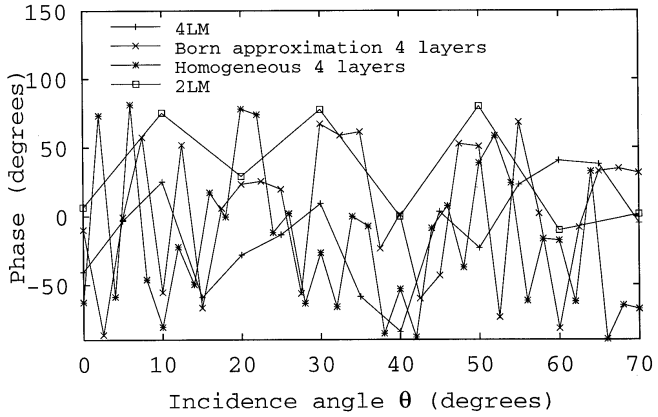

Figure 9. Phase of the reflected field, TE_x case, versus incidence angle for a 6 years old tree when the incident polarization is vertical.

20 MHz the corresponding wavelengths decrease, and the dimensions of the main scatterers (trunks) increase with respect to the wavelength, as well as their contribution to the scattered field. On figure 10 we represent the variations of R_{TM} versus frequency. The reflection coefficient is almost constant for the four models over the considered frequency range. The same behavior is observed for R_{TE_x}.

From the previously shown results, it appears that, the approximated models (Born approximation and homogeneous) give

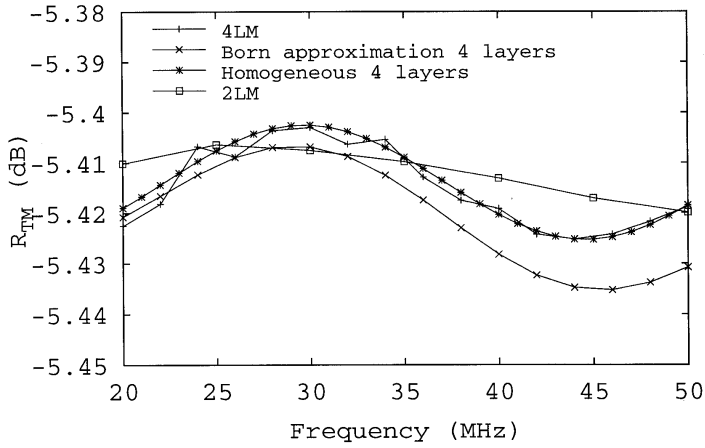

Figure 10. Modulus of the reflected field, R_{TM}, versus frequency, for a 6 years old tree.

good estimation of the specular reflection coefficient R, and since they allow lower computing time, we consider that they can be used to investigate the diffracted field by older trees which otherwise requires a more dense discretization and consequently leads to a larger computational time. The results obtained on Figure 10 show also that those models are still valid for higher frequencies.

4.2. Influence of the Age of the Trees

In this part we focus our analysis on the influence of the age of a forested area on the diffracted field. Considering the previous results, we chose the Born approximation to calculate this field with a reasonable computing time, especially for older trees (46 years old). In the results presented below we compute R by means of (13) and (15) where the numerator is replaced by the field diffracted by the trees only (we do not add the specular reflection of the multilayered medium). Then, we can easily observe the sensitivity of the response to the age of the illuminated forested area. In Figs. 11 to 13 we represent the variations of the diffracted field, versus the incidence angle, for different ages of the trees (6 to 46 years old). The frequency of the incident wave is 20 MHz for all cases of polarization. By considering those variations we can notice that the the coefficient R_{TM} is the most sensitive, at a given incidence, to the variation of the age of the forest.

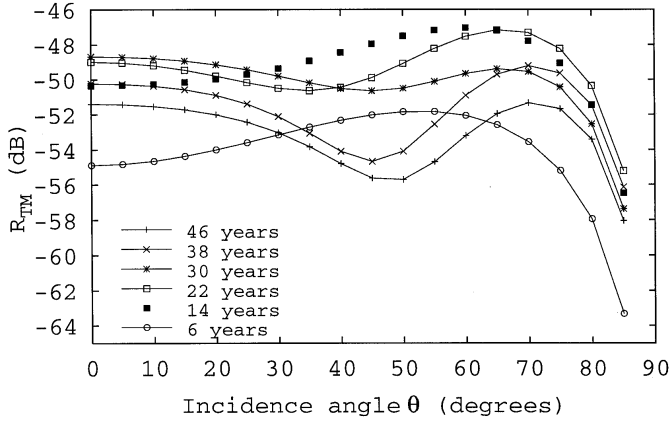

Figure 11. Modulus of the reflected field, R_{TM}, versus incidence angle, for a 6 to 46 years old tree.

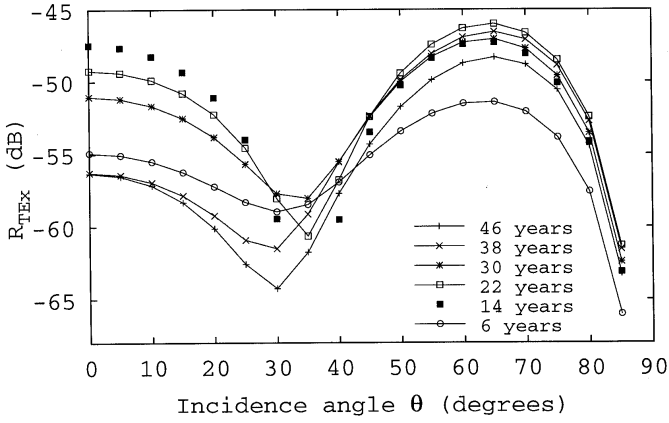

Figure 12. Modulus of the reflected field, R_{TE_x}, versus incidence angle, for a 6 to 46 years old tree.

4.3. Influence of the Representation of the Trees

In this part we focus our attention on the representation of the trees, so as to analyze the influence of each element making up the reference pattern of the grating at a given frequency (20 MHz) and age (46 years old). The considered model is the 2LM, solved by using the Born approximation. For this model the reference pattern is given in Fig. 2. We use here a more detailed representation by considering a

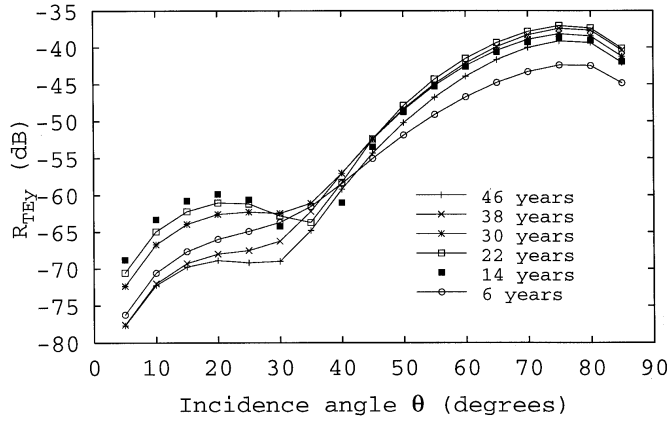

Figure 13. Modulus of the reflected field, R_{TE_y}, versus incidence angle, for a 6 to 46 years old tree.

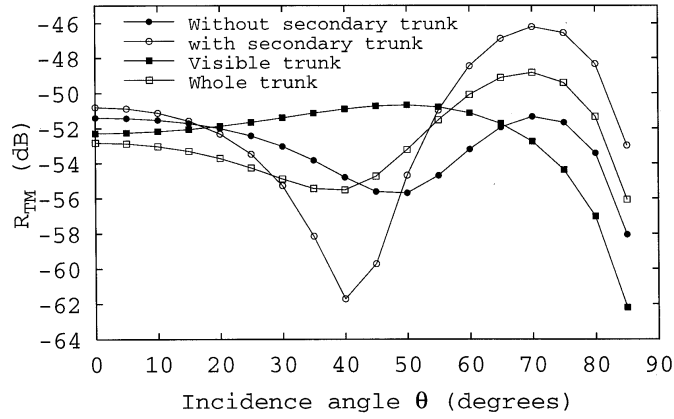

Figure 14. Modulus of the reflected field, R_{TM}, versus incidence angle, for a 6 to 46 years old tree, for different representations of the trees.

secondary trunk penetrating the foliage (see Fig. 2(b)). In Fig. 14 we represent the response R_{TM} obtained for four different representations of the elementary pattern with respect to the angle of incidence θ. The first and the second one are for the trees presented in Fig. 2(a) and 2(b). The third and fourth representations are obtained by removing the foliage from the trees of the previous cases. Thus, we consider respectively only the primary trunk (called visible trunk) and the

primary plus the secondary trunk (called whole trunk). The interest of this choice is to point out the coupling between the foliage (high part of the trees) and the primary trunk. The first remark is that each representation give a different response. But we notice that the variations of R_{TM} obtained for the third representation is the most detached from the other representations. Especially when we consider incidences greater than 40 degrees. It means that the interaction between the primary trunk and the upper layer must be considered to have a good representation of the trees.

5. CONCLUSION

Considering tile forest as an infinite array of trees is certainly a limitation of the present models. On an other hand these preliminary results show the efficiency of the integral representation of the electric field at low frequency, its ability to provide phase information and to take into account arbitrary linear polarization. We show also that the first-order Born's approximation, is valid for the analysis of forest backscattering at low frequencies. Work is going on to extend the present models to the case of forest of finite size.

APPENDIX A. THE DYADIC GREEN'S FUNCTION FOR THE 2LM AND THE 4LM

We give here the components of the dyads $\overline{\overline{g}}_{i\ 2lm}$ and $\overline{\overline{g}}_{i\ 4lm}$ which are used to obtain the periodic Green's functions given in (5). In the relations given below, the index i of $\overline{\overline{g}}_{i\ lm}$ indicates the layer in which we define $\overline{\overline{g}}_{lm}$ When we consider the 2LM i is equal to 1 ($y < 0$) or 2 ($y > 0$) and for the 4LM i varies between 1 and 4.

A.1. The Dyadic Green's Function for the 2LM

$$
\begin{aligned}
g_1^{xx}{}_{2lm}(\nu,\eta,y,y') &= C_1\Big\{ \exp j\gamma_1|y-y'| \\
&\quad +K_{12}\exp -j\gamma_1(y+y')\Big\} && \text{(A1)}\\
g_2^{xx}{}_{2lm}(\nu,\eta,y,y') &= C_2\exp -j\gamma_1 y' \exp j\gamma_2 y && \text{(A2)}\\
g_1^{yx}{}_{2lm}(\nu,\eta,y,y') &= C_3\exp -j\gamma_1(y'+y) && \text{(A3)}\\
g_2^{yx}{}_{2lm}(\nu,\eta,y,y') &= C_3\exp -j\gamma_1 y' \exp j\gamma_2 y && \text{(A4)}\\
g_1^{zx}{}_{2lm}(\nu,\eta,y,y') &= g_2^{zx}{}_{2lm}(\nu,\eta,y,y') = 0 && \text{(A5)}\\
g_1^{xy}{}_{2lm}(\nu,\eta,y,y') &= g_2^{xy}{}_{2lm}(\nu,\eta,y,y') = 0 && \text{(A6)}
\end{aligned}
$$

$$
\begin{aligned}
g_1^{yy}{}_{2lm}(\nu,\eta,y,y') &= C_1\Big\{\exp j\gamma_1|y-y'| \\
&\quad +K_{12}^{\epsilon}\exp -j\gamma_1(y+y')\Big\} && \text{(A7)}\\
g_2^{yy}{}_{2lm}(\nu,\eta,y,y') &= C_4\exp -j\gamma_1 y'\exp j\gamma_2 y && \text{(A8)}\\
g_1^{zy}{}_{2lm}(\nu,\eta,y,y') &= g_2^{zy}{}_{2lm}(\nu,\eta,y,y')=0 && \text{(A9)}\\
g_1^{xz}{}_{2lm}(\nu,\eta,y,y') &= g_2^{xz}{}_{2lm}(\nu,\eta,y,y')=0 && \text{(A10)}
\end{aligned}
$$

by replacing C_3 by C_5 we have:

$$
\begin{aligned}
g_1^{yz}{}_{2lm}(\nu,\eta,y,y') &= g_1^{yx}{}_{2lm}(\nu,\eta,y,y') \\
\text{and } g_2^{yz}{}_{2lm}(\nu,\eta,y,y') &= g_2^{yx}{}_{2lm}(\nu,\eta,y,y') && \text{(A11)}\\
g_1^{zz}{}_{2lm}(\nu,\eta,y,y') &= g_1^{xx}{}_{2lm}(\nu,\eta,y,y') && \text{(A12)}\\
g_2^{zz}{}_{2lm}(\nu,\eta,y,y') &= g_2^{xx}{}_{2lm}(\nu,\eta,y,y') && \text{(A13)}
\end{aligned}
$$

with

$$
\begin{aligned}
\gamma_i &= \sqrt{k_i^2-4\pi^2(\nu^2+\eta^2)},\quad K_{12}=\frac{\gamma_1-\gamma_2}{\gamma_1+\gamma_2}\\
K_{12}^{\epsilon} &= \frac{\gamma_1\epsilon_2-\gamma_2\epsilon_1}{\gamma_1\epsilon_2+\gamma_2\epsilon_1},\quad C_1=\frac{j}{2\gamma_1},\quad C_2=\frac{j}{\gamma_1+\gamma_2}\\
C_3 &= \frac{j2\pi\nu(\epsilon_2-\epsilon_1)}{(\gamma_1+\gamma_2)(\gamma_1\epsilon_2+\gamma_2\epsilon_1)},\quad C_4=\frac{j\epsilon_2}{\gamma_1\epsilon_2+\gamma_2\epsilon_1}\\
\text{and } C_5 &= \frac{j2\pi\eta(\epsilon_2-\epsilon_1)}{(\gamma_1+\gamma_2)(\gamma_1\epsilon_2+\gamma_2\epsilon_1)}. && \text{(A14)}
\end{aligned}
$$

A.2. The Dyadic Green's Function for the 4LM

The Dyadic Green's function for the 4LM is given in [19].

APPENDIX B. ELEMENTS OF THE MATRIX $[I^{KJ}]$

In the relations given below, i is the layer including the scatterers. That way, when we consider the 2LM i is equal to 1 and for the 4LM we have $i=3$.

$$
[I^{kj}]=\begin{bmatrix} I_{11}(k,j) & I_{12}(k,j) & I_{13}(k,j)\\ I_{21}(k,j) & I_{22}(k,j) & I_{23}(k,j)\\ I_{31}(k,j) & I_{32}(k,j) & I_{33}(k,j)\end{bmatrix} \qquad \text{(B1)}
$$

with

$$
I_{11}(k,j) = \Delta\epsilon_i(r_k)\left\{\left(k_i^2+\frac{\partial^2}{\partial x_j^2}\right)\tilde{g}^{xx}(k,j)+\frac{\partial^2\tilde{g}^{yx}(k,j)}{\partial x_j\partial y_j}\right\} \qquad \text{(B2)}
$$

$$I_{12}(k,j) = \Delta\epsilon_i(r_k)\frac{\partial^2\tilde{g}^{yy}(k,j)}{\partial x_j \partial y_j} \quad \text{(B3)}$$

$$I_{13}(k,j) = \Delta\epsilon_i(r_k)\left\{\frac{\partial^2\tilde{g}^{zz}(k,j)}{\partial x_j \partial z_j} + \frac{\partial^2\tilde{g}^{yz}(k,j)}{\partial x_j \partial y_j}\right\} \quad \text{(B4)}$$

$$I_{21}(k,j) = \Delta\epsilon_i(r_k)\left\{\frac{\partial^2\tilde{g}^{xx}(k,j)}{\partial y_j \partial x_j} + \left(k_i^2 + \frac{\partial^2}{\partial y_j^2}\right)\tilde{g}^{yx}(k,j)\right\} \quad \text{(B5)}$$

$$I_{22}(k,j) = \Delta\epsilon_i(r_k)\left(k_i^2 + \frac{\partial^2}{\partial y_j^2}\right)\tilde{g}^{yy}(k,j) \quad \text{(B6)}$$

$$I_{23}(k,j) = \Delta\epsilon_i(r_k)\left\{\frac{\partial^2\tilde{g}^{zz}(k,j)}{\partial y_j \partial z_j} + \left(k_i^2 + \frac{\partial^2}{\partial y_j^2}\right)\tilde{g}^{yz}(k,j)\right\} \quad \text{(B7)}$$

$$I_{31}(k,j) = \Delta\epsilon_i(r_k)\left\{\frac{\partial^2\tilde{g}^{xx}(k,j)}{\partial z_j \partial x_j} + \frac{\partial^2\tilde{g}^{yx}(k,j)}{\partial z_j \partial y_j}\right\} \quad \text{(B8)}$$

$$I_{32}(k,j) = \Delta\epsilon_i(r_k)\frac{\partial^2\tilde{g}^{yy}(k,j)}{\partial z_j \partial y_j} \quad \text{(B9)}$$

$$I_{33}(k,j) = \Delta\epsilon_i(r_k)\left\{\left(k_i^2 + \frac{\partial^2}{\partial z_j^2}\right)\tilde{g}^{zz}(k,j) + \frac{\partial^2\tilde{g}^{yz}(k,j)}{\partial z_j \partial y_j}\right\} \quad \text{(B10)}$$

where

$$\tilde{g}^{uv}(k,j) = \frac{1}{\Delta x \Delta z}\sum_{m=-\infty}^{+\infty}\sum_{n=-\infty}^{+\infty}\iint_{\Omega_j} g^{uv}(\nu_n,\eta_m,y_k,y_j) \times \exp j2\pi(\nu_n(x_k - x_j) + \eta_m(z_k - z_j))dr_j \quad \text{(B11)}$$

REFERENCES

1. Le Toan, T., A. Beaudoin, J. Riom, and D. Guyon, "Relating forest biomass to SAR data," *IEEE Transaction on Geoscience and Remote Sensing,* Vol. 30, No. 2, 403–411, 1992.
2. Israelsson, H., J. Askne, and R. Sylvander, "Potential of SAR for forest biomass to SAR data," *International Journal of Remote Sensing,* Vol. 15, No. 14, 2809–2826, 1994.
3. Dobson, G., T. Ulaby, T. Le Toan, A. Beaudoin, E. Kasischke, and N. Christensen, "Dependence of radar backscatter on coniferous forest biomass," *IEEE Transaction on Geoscience and Remote Sensing,* Vol. 30, No. 2, 412–415, 1992.
4. Paloscia, S., G. Macelloni, P. Pampaloni, and S. Sigismondi, "The potential of C- and L- band SAR in estimating vegetation biomass:

The ER.S-1 and JERS-1 experiments," *IEEE Transaction on Geoscience and Remote Sensing,* Vol. 37, No. 4, 2107–2110, 1999.

5. Gustavsson, A., H. Hellsten, B. Larsson, and L. Ulander, "Development and operation of the FOA CARABAS VHF-SAR system," *Proceedings of PIERS,* Nantes, 1998.
6. Hellsten, H., P. Frlind, A. Gustavsson, T. Jonsson, B. Larsson, G. Stenstrm, B. Binder, M. Mirkin, and S. Ayasli, "Ultra-wideband VHF SAR-design and measurements," *Proceedings of SPIE,* Orlando, 1994.
7. Hellsten, H., L. Ulander, A. Gustavsson, and B. Larsson, "Development of VHF CAR.ABAS II SAR.," *Proceedings of SPIE Conf. Radar Sensor Technology,* Orlando, 1996.
8. Hsu, C., H. Han, H. Shin, R. Kong, J. Beaudoin, and T. Le Toan, "Radiative transfer theory for polarimetric remote sensing of pine forest at P-band," *International Journal of Remote Sensing,* Vol. 15, No. 14, 2943–2954, 1994.
9. Israelsson, H., L. M. H. Ulander, T. Martin, and J. Askne, "A coherent scattering model to determine forest backscattering in the VHF-Band," *IEEE Transaction on Geoscience and Remote Sensing,* Vol. 38, No. 1, 238–248, 2000.
10. Beaudoin, J., T. Le Toan, S. Goze, E. Goze, E. Nezry, A. Lopez, E. Mougin, C. Hsu, H. Han, J. Kong, and R. Shin, "Retrieval of forest biomass from SAR data," *International Journal of Remote Sensing,* Vol. 15, No. 14, 2777–2796, 1994.
11. Torgovrlikov, *Dielectric Properties of Wood an Wood-Based Materials,* Springer-Verlag, 1993.
12. Peplinski, N., F. Ulaby, and M. Dobson, "Dielectric properties of soils in the 0.3–1.3 GHz range," *IEEE Transaction on Geoscience and Remote Sensing,* Vol. 33, No. 3, 803–807, 1995.
13. Ulaby, F., R. Moore, and A. Fung, *Microwave Remote Sensing: Active and Passive,* Vol. 3, Artech House, 1986.
14. Chew, W. C., *Waves and Fields in Inhomogeneous Media,* IEEE-Press, 1995.
15. Richmond, J., "Scattering by a dielectric cylinder of arbitrary cross section shape," *IEEE Transaction on Antennas and Propagation,* Vol. 13, No. 3, 334–341, 1965.
16. Richmond, J., "TE-wave scattering by a dielectric cylinder of arbitrary cross-section shape," *IEEE Transaction on Antennas and Propagation,* Vol. 14, No. 4, 460–464, 1966.
17. Su, C.-C., "A simple evaluation of some principal value integrals for dyadic Green's function using symmetry property," *IEEE*

Transaction on Antennas and Propagation, Vol. 35, No. 11, 1306–1307, 1987.

18. Singh, S., W. Richards, J. Zinecker, and D. Wilton, "Accelerating the convergence of series representing the free space periodic Green's function," *IEEE Transaction on Antennas and Propagation,* Vol. 38, No. 12, 1958–1962, 1990.
19. Angot, L., "Modélisation de l'interaction d'une onde électromagnétique avec un objet: application a l'observation d'une forêt dans le domaine des fréquences VHF," Ph.D. thesis, Université Pierre et Marie Curie, 1999.